Archive of Applied Mechanics (2022) 92:1529–1549
https://doi.org/10.1007/s00419-022-02128-y

ORIGINAL

M. E. Nasr · Ahmed E. Abouelregal

Light absorption process in a semiconductor infinite body with a cylindrical cavity via a novel photo-thermoelastic MGT model

Received: 4 August 2021 / Accepted: 25 January 2022 / Published online: 9 March 2022
© The Author(s), under exclusive licence to Springer-Verlag GmbH Germany, part of Springer Nature 2022

Abstract Photothermal spectroscopy is a method of measuring the optical absorption and thermal properties of semiconductor materials using high-sensitivity spectroscopic techniques. Heating occurs due to light, which is absorbed but not dissipated by emission. In this paper, a new model is provided that can be used to understand the process of optical thermal transfer and the interaction between elastic plasma waves and heat. The proposed photothermal model is described by the Moore–Gibson–Thompson heat equation. Using the proposed model, the thermal and photoacoustic effects in an infinite isotropic and homogeneous body with a cylindrical cavity of semiconductor material crossed into a fixed magnetic field and subjected to high-intensity laser heat flux were investigated. The inner surface of the cavity is considered to be traction-free, and the carrier density is photogenerated by a laser pulse heat flux that decays exponentially. The numerical calculations for the components of thermal stresses, displacement, temperature field, and carrier density are obtained using the Laplace transform approach. The propagation of heat, elastic, and plasma waves, as well as the distributions of each investigated field, were examined and explained. The comparison is also used to see how different thermal response features, such as thermal relaxation, laser pulse duration, and lifetime, affect the thermoelastic response.

Keywords Photo-thermoelasticity · Semiconductor · Cylindrical cavity · Laser pulse heating

1 Introduction

Two events predicted by the conventional uncoupled thermoelasticity model do not correspond to the physical facts. First, there are no elastic components in this theory's heat conduction equation; second, the heat equation is of the parabolic type, implying that heat waves would propagate at limitless velocities. To solve the first weakness, Biot [1] proposed the idea of coupled thermoelasticity. This theory's governing equations are associated, which solves the classical theory's first contradiction. The heat equation for the coupled model is likewise parabolic; therefore, both theories suffer from the second flaw. Several researchers have proposed new formulations of thermoelasticity to replace the coupled Biot theory [1]. Since the heat equations associated with these models are hyperbolic, they immediately avoid the challenge of infinite propagation velocities found in both uncoupled and coupled thermoelastic models.

Using the Maxwell–Cattaneo law of heat conduction, Lord and Shulman [2] developed the theory of generalized thermoelasticity with one relaxation time for isotropic materials (labeled as the LS theory). Because this theory's heat equation is of the wave type, it assures that heat and elastic waves propagate at limited speeds.

M. E. Nasr · A. E. Abouelregal (✉)
Department of Mathematics, College of Science and Arts, Jouf University, Al-Qurayat, Saudi Arabia
e-mail: ahabogal@ju.edu.sa

A. E. Abouelregal
Basic Sciences Research Unit, Jouf University, Sakaka, Saudi Arabia

The rest of the governing equations for this theory, such as the equations of motion and constitutive relations, are identical to those for the coupled and uncoupled models. By proposing a novel thermoelastic inequality, Green and Lindsay [3] established the theory of thermoelasticity with two relaxation durations (named the GL model). Not only does this theory change the heat equation, but it also changes the equations of the associated theory. When the medium under examination has a center of symmetry, the classical Fourier equation of heat conduction is not disturbed.

Green and Naghdi [4–6] made sufficient changes to the constitutive equations to allow consideration of a noticeably larger class of heat flow problems known as GN-I, GN-II, and GN-III. The independent constitutive variables in GN models contain a phrase termed "thermal displacement gradient". When the different theories are linearized, GN-I's heat transport equation is identical to the classical heat equation, but GN-II and GN-III both allow for the transmission of finite-speed thermal signals [6]. The presence of a thermal damping component in the GN-III theory allows heat energy to be dissipated. Additional contributions to this theory can be detected in [7–12].

The Moore-Gibson-Thompson (MGT) equation has grown more important in recent years, as evidenced by numerous academic articles devoted to its study and interpretation. The theory was founded on a third-order differential equation, which is crucial to many fluid dynamics [13]. Quintanilla [14, 15] is constructing a novel heat conduction model under the MGT equation. Abouelregal et al. [16–18] prepared the proposed modified heat equation after adding the relaxation parameter in the GN-III model and using the energy equation. The number of articles on this theory has been greatly increased since the advent of the MGT equation [19–22].

Some materials, such as semiconductors, offer a variety of physical characteristics that are useful during research. According to the principle of thermoelasticity, semiconductor materials may only be classed as elastic materials. The relevance of semiconductors in current technology was recently highlighted when they were utilized to produce electrical energy from sunlight while also being subjected to laser pulses [23]. Semiconductor materials are utilized as nanomaterials in various fields of mechanical and electrical engineering, and they have a variety of uses in modern industry, including transistors, screens, and solar cells. The photothermal theory has recently been applied to semiconductor media to produce sustainable energy technologies. Several mathematical-physical models were studied to characterize the overlap between the photothermal equations and the thermoelasticity equations. Gordon et al. [24] first introduced electronic deformations to photothermal spectroscopy. While using a laser source, photoacoustic spectroscopy is utilized in the context of sensitive analytical procedures to measure the velocity of sound of some semiconductor materials [25]. Many applications in current engineering industries employ wave propagation during electro-deformations of semiconductor medium in photothermal processing techniques [26–34].

The sample is regularly elastically and electro-deformed by the photo-excited carriers. The mechanism for electronic deformation is founded on the fact that photogenerated plasma in the semiconductor produces crystal lattice deformation, i.e., deformation of the conductive potential and valence strips in the semiconductor. This can result in local stress in the sample via photo-stimulated carriers. This strain in turn can create plasma waves in the semiconductor by regular elastic local similar to thermal wave production [35].

The damage caused by laser use of optical materials is a distinct area. For more than 50 years, several publications have attempted to address the topic from a theoretical and experimental standpoint. Because pulsed laser technologies are widely used in material processing and non-destructive detection and characterization, the excitation of thermoelastic waves by a pulsed laser in solids is of significant interest. When a solid absorbs a laser pulse, it creates a localized temperature rise, which induces thermal expansion and forms a thermoelastic wave in the material. Two influences become significant in ultra-short pulsed laser heating [36]. A high-powered focused laser beam may heat materials to thousands of degrees Kelvin. The temperature of continuous-wave laser heating may be monitored remotely with great precision by fitting the spectrum irradiance to a blackbody curve. Heating using a pulsed laser offers several benefits, but the temperature increases and falls in nanoseconds, necessitating quick electronics and time-consuming methods to estimate the temperature [37].

Metal softening and/or hardness, annealing of crystalline or polycrystalline materials, diffusion of dopants in semiconductors, synthesis of compounds and thin films, polymerization of polymers, and other applications of laser heating are all possible. Thermally triggered processes, bulk diffusion, and phase transitions have all been aided by laser annealing. Laser heating has the benefit of being both spatially and temporally localized. Additionally, by establishing thermal gradients, sample temperatures considerably above the sample chamber's capacity can be obtained, such as heated samples in diamond anvil cells [38, 39].

Laser heating has a number of benefits over traditional techniques, including accuracy, local therapy, and low cost. Absorption occurs when a high-intensity laser interacts with a solid surface. As a result, the substrate material gains internal energy, and the irradiated zone releases heat. Since the process is often rapid, temperature

gradients in the irradiated zone remain considerable. As a result, there is a lot of thermal strain and thermally generated tension in this area. Furthermore, from the standpoint of application, the end result is critical in the laser treatment procedure. High stress levels in the irradiated zone may cause the surface to fail due to stress-induced cracking. As a result, caution must be exercised during the laser therapy procedure [40].

The mechanical, electric, and thermal properties of semiconductor materials vary with changes in temperature. When a temperature gradient due to the absorption of light occurs in semiconductor elastic materials, it causes an electric potential difference between endpoints in the semiconductor. Several authors have analyzed the uncoupled and coupled systems of plasma, thermodynamic, and elastic equations as well as the different effects of thermal as well as electronic deformation in semiconductors using classical models. According to a literature review, there is no work examining the photothermal interactions of semiconductor cylinders subjected to ultrashort pulsed laser heating and photogenerated plasmas, as well as the properties of temperature-dependent materials. The primary motivation for conducting a comprehensive examination of such issues in this study is the importance of the issue and its multiple applications. This theoretical study is also, like spectroscopic methods, one of the important experimental tools that are used to investigate the micro and macro properties of semiconductors.

When a semiconductor material sample is lit, pairs of superconductors are formed, which propagate through the material according to density gradients. Each pair carries about the same amount of energy as the material's band gap. As the surplus electron joins with the hole, the energy is deposited, causing local heating of the lattice. As a result, the temperature distribution in the sample will be calculated, which is based on the optical absorption, mass recombination, and surface features in and on the sample. The photothermal process is the development of a temperature field in a material using diffusion carriers and optically induced recombination. This study addresses the case of low temperature rises in an infinite solid cylinder and gives a formulation of the theory guiding the photothermal effect. This type of research, which is an extension of the optical diffraction approach, has significant benefits in that it directly determines both the thermal and electronic transport parameters within the semiconductor block as well as at the surface or interface. Another important benefit is the ability to physically calculate and evaluate these transport properties using a mathematical model.

The purpose of this paper is to investigate disturbances in infinite, isotropic, homogeneous thermoelastic semiconductor materials using the Moore-Gibson-Thompson (MGT) heat conduction equation. The propagation of waves in semiconductor materials has many applications in various fields of science and technology, namely atomic physics, industrial engineering, thermal power plants, submarine structures, pressure vessels, aerospace, chemical pipes, and metallurgy. The effect of thermo-electronic deformation in semiconductors has been investigated, including partially coupled plasma, thermal mechanisms, and elastic waves. We used the normal mode method analysis to solve a system of partial differential equations in this phenomenon under proper boundary conditions. Physical field quantities are introduced analytically and graphed, along with some analytical comparisons. The results obtained were compared with the results of the work of other researchers.

2 Basic equations

The generalized coupled hyperbolic plasma and generalized thermal and elastic equations, for thermoelastic semiconductors with isotropic and homogeneous electronic, thermal, and elastic properties are given by:

Equations of motion:

$$\sigma_{ij,j} + F_i = \varrho \ddot{u}_i \tag{1}$$

The constitutive equations:

$$\sigma_{ij} = C_{ijkl} e_{kl} - \left(\beta_{ij}\theta + d_{nij} N\right) \tag{2}$$

The strain–displacement relations:

$$e_{ij} = \frac{1}{2}\left(u_{i,j} + u_{j,i}\right) \tag{3}$$

In Eqs. (1)–(3), σ_{ij} are the stress components, ϱ is the density of the material, u_i are the displacement components, F_i are the body force components, and $i, j, k = 1, 2, 3$, e_{ij} is the strain tensor, $e_{kk} = e$ is the cubical dilatation, $d_{nij} = d_{ni}\delta_{ij}$ are the difference in deformation potential of the conduction and valence bands and C_{ijkl} are the elastic constants for material, $\beta_{ij} = \beta_i \delta_{ij}$ are the stress-temperature coefficients. Also,

$\theta = T - T_0$ denotes the thermodynamical temperature, T_0 is the reference temperature, and N is the carrier density.

The coupled plasma-thermal-elastic wave equation can be written as [27, 41]

$$\left(D_{Eij}N_{,j}\right)_{,i} = \varrho\frac{\partial N}{\partial t} + \frac{1}{\tau}N + \kappa\theta + G \tag{4}$$

where D_{Eij} are the diffusion coefficients, κ is the thermal activation coupling parameter, τ is the lifetime of photogenerated electron–hole pairs and G is the carrier photogeneration "source" term. In the case of harmonic modulation lasers, Vasilev and Sandomirskii [42] first found that the thermal activation coupling parameter κ is insignificant at low temperatures.

Cattaneo-Vernotte in [43–45] introduced a wider Fourier law by adding the thermal relaxation τ_0 to the vector of the heat flow $\vec{q}$ as

$$\left(1 + \tau_0\frac{\partial}{\partial t}\right)\vec{q} = -K_{ij}\vec{\nabla}\theta \tag{5}$$

In Eq. (1), K_{ij} refers to the thermal conductivity tensor.

The improved Fourier law based on the GN-III model can be represented as [6]

$$\vec{q} = -K_{ij}\,\vec{\nabla}\theta - K^*_{ij}\vec{\nabla}\vartheta \tag{6}$$

where the function ϑ denotes thermal displacement which satisfies $\dot{\vartheta} = \theta$ and the parameters K^*_{ij} refer to the thermal conductivity rates. The equation for the energy balance can be written as [10, 46]

$$\varrho C_E\frac{\partial\theta}{\partial t} + T_0\frac{\partial}{\partial t}\left(\beta_{ij}e_{ij}\right) = -\vec{\nabla}\cdot\vec{q} + Q \tag{7}$$

where C_E is the specific heat at constant volume, Q is the heat source.

The combination of the improved Fourier law proposed in (6) with the energy Eq. (7) has the same weakness as Fourier's normal theory, predicting that thermal waves are spreading immediately. Quintanilla [14, 15] and Abouelregal et al. [16–18] prepared the proposed modified heat equation after adding the relaxation parameter in the GN-III model. The modified Fourier's law would then take the following form [14, 15]

$$\left(1 + \tau_0\frac{\partial}{\partial t}\right)\vec{q} = -K_{ij}\,\vec{\nabla}\theta - K^*_{ij}\vec{\nabla}\vartheta \tag{8}$$

Consider that the semiconductor elastic medium is subjected to light beams from the outside and that the excited free electrons create a carrier-free charge density with semiconductor gap energy E_g. Because of the absorbed optical energy, there is a change in electronic deformation and elastic vibrations. Thermal-elastic-plasma waves will affect the overall form of the heat conductivity equation in this situation. The modified Fourier law for semiconductor materials with plasma effects in a generalized version can be written as follows:

$$\left(1 + \tau_0\frac{\partial}{\partial t}\right)\vec{q} = -K_{ij}\,\vec{\nabla}\theta - K^*_{ij}\vec{\nabla}\vartheta - \int\frac{E_g}{\tau}\frac{\partial N}{\partial t}d\vec{x} \tag{9}$$

The photo-excitation effect is represented by the final term in Eq. (9). When the above equation is differentiated with respect to $\vec{x}$, the result is

$$\left(1 + \tau_0\frac{\partial}{\partial t}\right)\left(\vec{\nabla}\cdot\vec{q}\right) = -\vec{\nabla}\cdot\left(K_{ij}\,\vec{\nabla}\theta\right) - \vec{\nabla}\cdot\left(K^*_{ij}\vec{\nabla}\vartheta\right) - \frac{E_g}{\tau}\frac{\partial N}{\partial t} \tag{10}$$

By substituting Eq. (10) into Eq. (7), the modified heat conduction equation with thermal memory that explains the interaction between the thermal-plasma-elastic waves may be derived as

$$\left(1 + \tau_0\frac{\partial}{\partial t}\right)\left[\varrho C_E\frac{\partial^2\theta}{\partial t^2} + T_0\frac{\partial^2}{\partial t^2}\left(\beta_{ij}u_{i,j}\right) - \varrho\frac{\partial Q}{\partial t}\right] = \left(K_{ij}\dot{\theta}_{,j}\right)_{,i} + \left(K^*_{ij}\theta_{,j}\right)_{,i} + \frac{E_g}{\tau}\frac{\partial^2 N}{\partial t^2} \tag{11}$$

We assume that the adjacent free space is permeated by an initial magnetic field $\vec{H}$. This generates an induced electro-field $\vec{E}$ and induced magnetic field $\overrightarrow{h}$ that fulfills the magnetic equations of Maxwell and is sufficient for slowly moving media:

$$\vec{J} = \nabla \times \vec{h}, \nabla \times \vec{E} = -\mu_0 \frac{\partial \vec{h}}{\partial t}, \vec{E} = -\mu_0 \left(\frac{\partial \vec{h}}{\partial t} \times \vec{H} \right), \nabla \cdot \vec{h} = 0 \tag{12}$$

$$\tau_{ij} = \mu_0 \left[H_i h_j + H_j h_i - H_k h_k \delta_{ij} \right] \tag{13}$$

where μ_0 is the magnetic permeability, $\vec{J}$ is the current density and τ_{ij} is the Maxwell stress tensor.

3 Formulation of the problem

In this section, wave propagation on a cylindrical cavity semiconductor material during the photo-thermo-elastic process is investigated using the constructed combined plasma, thermal, and elastic wave model. It was thought to use an infinite material, which is an elastic semiconductor with a cylindrical cavity, and thermoelastic, isotropic, and uniform properties. Decreasing the heat flux of the laser pulse resulted in photogeneration of carrier density, which is confined to the inner surface of the cavity.

The cylindrical coordinates (ρ, ϕ, z) with the z-axis aligned along the cylinder axis are considered. Due to symmetry, the semiconductor medium with a cylindrical cavity is assumed to cover the area $\rho_0 \leq \rho < \infty$, and its state may be described in terms of the time t and distance ρ. Initially, the temperature in the cylinder is steady and uniform T_0. Furthermore, for the regularity constraint, all physical field variables are assumed to be finite within the medium.

The only non-vanishing displacement components and displacement–strain relations are

$$u_\rho = u(\rho, t), e_{\rho\rho} = \frac{u}{\rho}, e_{\phi\phi} = \frac{\partial u}{\partial \rho} \tag{14}$$

The stress–strain-temperature-carrier relations (2) will be the form

$$\begin{aligned} \sigma_{\rho\rho} &= 2\mu \frac{\partial u}{\partial \rho} + \lambda e - (3\lambda + 2\mu)(\alpha_t \theta + \delta_n N), \\ \sigma_{\phi\phi} &= 2\mu \frac{u}{\rho} + \lambda e - (3\lambda + 2\mu)(\alpha_t \theta + \delta_n N), \\ \sigma_{zz} &= \lambda e - (3\lambda + 2\mu)(\alpha_t \theta + \mathrm{d}_n N) \end{aligned} \tag{15}$$

where α_t is the linear thermal expansion coefficient, δ_n is the electronic deformation coefficient, λ, μ are the Lame's constants, and $e = \frac{1}{\rho} \frac{\partial(\rho u)}{\partial \rho}$. When the Lorentz force F_ρ is taken into account, the dynamic motion equation becomes

$$\frac{\partial \sigma_{\rho\rho}}{\partial \rho} + \frac{1}{\rho} \left(\sigma_{\rho\rho} - \sigma_{\phi\phi} \right) + F_\rho = \varrho \frac{\partial^2 u}{\partial t^2} \tag{16}$$

Assume the cylinder is immersed in a magnetic field of constant strength $\overrightarrow{H}_0 = (0,\ 0,\ H_0)$. According to Eq. (12), we obtain

$$\vec{E} = \left(0,\ \mu_0 H_0 \frac{\partial u}{\partial t},\ 0 \right),\ \vec{J} = \left(0,\ \frac{\partial}{\partial \rho} \left(\frac{1}{\rho} \frac{\partial(\rho u)}{\partial \rho} \right),\ 0 \right),\ \vec{h} = \left(0,\ 0,\ \frac{1}{\rho} \frac{\partial(\rho u)}{\partial \rho} \right) \tag{17}$$

The magnetic field $\vec{H}_0$ induces the radial component of the Lorentz force F_ρ, which is given by

$$F_\rho = \mu_0 \left(\vec{J} \times \vec{H}_0 \right)_\rho \tag{18}$$

Thus, we have F_ρ and Maxwell's stress $\tau_{\rho\rho}$ from Eqs. (13) and (17) as

$$F_r = \mu_0 H_0^2 \frac{\partial}{\partial \rho} \left(\frac{1}{\rho} \frac{\partial(\rho u)}{\partial \rho} \right), \quad \tau_{\rho\rho} = \mu_0 H_0^2 \frac{1}{\rho} \frac{\partial(\rho u)}{\partial \rho} \tag{19}$$

Inserting Eqs. (15) and (19) into Eq. (16), then we have

$$\left(\lambda+2\mu+\mu_0 H_0^2\right)\frac{\partial}{\partial\rho}\left(\frac{1}{\rho}\frac{\partial(\rho u)}{\partial\rho}\right)-\gamma\frac{\partial\theta}{\partial\rho}-d_n\frac{\partial N}{\partial\rho}=\varrho\frac{\partial^2 u}{\partial t^2} \tag{20}$$

where $\{\gamma, d_n\}=(3\lambda+2\mu)\{\alpha_t, \delta_n\}$.

When we apply the operator $\frac{1}{\rho}\frac{\partial(\rho u)}{\partial\rho}$ to both sides of Eq. (20), we obtain

$$\left(\lambda+2\mu+\mu_0 H_0^2\right)\nabla^2 e-\gamma\nabla^2\theta-d_n\nabla^2 N=\varrho\frac{\partial^2 e}{\partial t^2} \tag{21}$$

In the cylindrical coordinate system, the Laplacian operator is given by $\nabla^2=\frac{\partial^2}{\partial\rho^2}+\frac{1}{\rho}\frac{\partial}{\partial\rho}$. Without any heat sources ($Q=0$), the generalized modified MGTE heat conduction Eq. (11) will be as follows:

$$\left(1+\tau_0\frac{\partial}{\partial t}\right)\left[\varrho C_E\frac{\partial^2\theta}{\partial t^2}+\gamma T_0\frac{\partial^2 e}{\partial t^2}\right]=K\nabla^2\dot{\theta}+K^*\nabla^2\theta+\frac{E_g}{\tau}\frac{\partial^2 N}{\partial t^2} \tag{22}$$

The governing equations can easily be transformed into dimensionless forms. As a result, the dimensionless variables listed below are presented:

$$\begin{gathered}\left\{\rho', u'\right\}=v_0\eta\{\rho, u\}, \left\{t', \tau_0', \tau'\right\}=v_0^2\eta\{t, \tau_0, \tau\}, \left\{\theta', N'\right\}=\frac{1}{\rho v_0^2}\{\gamma\theta, d_n n\},\\ \left\{\sigma_{ij}', \tau_{\rho\rho}'\right\}=\frac{1}{\rho v_0^2}\{\sigma_{ij}, \tau_{\rho\rho}\}, \eta=\frac{\rho C_E}{K}, v_0^2=v_1^2+v_a^2\end{gathered} \tag{23}$$

In Eq. (23), the parameter $v_1=\sqrt{\frac{\lambda+2\mu}{\varrho}}$ represents the dilatational wave speed, and the factor $v_a=\sqrt{\frac{\mu_0 H_0^2}{\varrho}}$ symbolizes the medium Alfven wave speed. The governing equations can be rewritten in the following forms if the primes are ignored:

$$\left(1+\tau_0\frac{\partial}{\partial t}\right)\left[\frac{\partial^2\theta}{\partial t^2}+\varepsilon_1\frac{\partial^2 e}{\partial t^2}\right]=\left(\frac{\partial}{\partial t}+\omega^*\right)\nabla^2\theta+\varepsilon_2\frac{\partial^2 N}{\partial t^2} \tag{24}$$

$$\nabla^2 e-\nabla^2\theta-\nabla^2 N=\frac{\partial^2 e}{\partial t^2} \tag{25}$$

$$\nabla^2 N=g_1\frac{\partial N}{\partial t}+g_2 N+g_3\theta \tag{26}$$

$$\begin{aligned}\sigma_{\rho\rho}&=2\beta^2\frac{\partial u}{\partial\rho}+\left(1-2\beta^2\right)e-\theta-N,\\ \sigma_{\phi\phi}&=2\beta^2\frac{u}{\rho}+\left(1-2\beta^2\right)e-\theta-N,\\ \sigma_{zz}&=\left(1-2\beta^2\right)e-\theta-N\end{aligned} \tag{27}$$

where

$$\begin{gathered}\beta^2=\frac{\mu}{\lambda+2\mu},\ \varepsilon_1=\frac{\gamma^2 T_0}{\rho^2 C_e c_0^2},\ \omega^*=\frac{K^*}{c_0^2 K},\ \varepsilon_2=\frac{\gamma E_g v_0^2\eta}{\tau d_n\varrho C_E},\\ \eta_0=(c_0\eta)^2,\ g_1=\frac{\rho}{D_E\eta_0},\ g_2=\frac{1}{D_E\eta_0\tau_1},\ g_3=\frac{\kappa d_n}{\gamma D_E\eta_0}\end{gathered} \tag{28}$$

The initial conditions of the problem are taken as

$$\begin{aligned}&u(\rho,0)=0=\frac{\partial u(\rho,0)}{\partial\rho}, N(\rho,0)=0=\frac{\partial N(\rho,0)}{\partial\rho},\\ &\theta(\rho,0)=0=\frac{\partial\theta(\rho,0)}{\partial\rho}\end{aligned} \tag{29}$$

We suppose that the cylinder's interior surface is traction-free. Then the mechanical boundary conditions in this case can be expressed as

$$\sigma_{\rho\rho}(\rho, t) = 0 \quad \text{at } \rho = \rho_0 \tag{30}$$

Also, we assume that a variable heat flux in the form of exponentially laser pulsed heat is applied to the boundary surface $\rho = \rho_0$. As a result, the following boundary condition may be applied [47]:

$$q_\rho = q_0 \frac{t^2}{16t_p^2} e^{-t/t_p}, \quad \text{at} \quad \rho = \rho_0 \tag{31}$$

where q_0 is a constant and t_p is the pulsing heat flux duration time.

Using the modified Fourier's Law (8), after using dimensionless variables (23), there will be

$$\left(1 + \tau_0 \frac{\partial}{\partial t}\right)\dot{q}_\rho = -\left(\frac{\partial}{\partial t} + \omega^*\right)\frac{\partial \theta}{\partial \rho} \tag{32}$$

Equations (31) and (32) are decoupled to provide the following boundary condition:

$$\frac{q_0}{16t_p^2}\left(1 + \tau_0 \frac{\partial}{\partial t}\right)\frac{\partial}{\partial t}\left(t^2 e^{-t/t_p}\right) = -\left(\frac{\partial}{\partial t} + \omega^*\right)\frac{\partial \theta}{\partial \rho} \text{ at } \rho = \rho_0 \tag{33}$$

The carriers can reach the sample surface during the diffusion phase, with a finite probability of recombination. As a result, the carrier density boundary condition may be written as follows:

$$D_E \frac{\partial N}{\partial \rho} = s_v N \quad \text{at} \quad \rho = \rho_0 \tag{34}$$

where s_v is the surface recombination velocity.

4 Solution in the domain of the Laplace transform

The Laplace transform is utilized for solving linear differential equations with constant coefficients. In control system engineering, the Laplace transformation is very important. Laplace transforms of various functions must be performed to examine the control system. In order to analyze the dynamic control system, both the characteristics of the Laplace transform and the inverse Laplace transformation are employed. The Laplace transform of a function $g(t)$, which is denoted by $\mathcal{L}[g(t)]$ or by $\overline{g}(s)$, is defined by the following equation:

$$\mathcal{L}[g(t)] = \overline{g}(s) = \int_0^\infty g(t) e^{-st} \mathrm{d}t, s > 0 \tag{35}$$

We get the following results by using the Laplace transform approach to Eqs. (24)–(27):

$$\left(\nabla^2 - \psi\right)\overline{\theta} = \psi \varepsilon_1 \overline{e} - \varepsilon_2 s^2 \overline{N} \tag{36}$$

$$\left(\nabla^2 - s^2\right)\overline{e} = \nabla^2 \overline{\theta} + \nabla^2 \overline{N} \tag{37}$$

$$\left(\nabla^2 - g_4\right)\overline{N} = g_3 \overline{\theta} \tag{38}$$

$$\begin{bmatrix} \overline{\sigma}_{\rho\rho} \\ \overline{\sigma}_{\phi\phi} \\ \overline{\sigma}_{zz} \end{bmatrix} = \begin{bmatrix} 2\beta^2 & 0 & \left(1 - 2\beta^2\right) & -1 & -1 \\ 0 & 2\beta^2 & \left(1 - 2\beta^2\right) & -1 & -1 \\ 0 & 0 & \left(1 - 2\beta^2\right) & -1 & -1 \end{bmatrix} \begin{bmatrix} \frac{\partial \overline{u}}{\partial \rho} \\ \frac{\overline{u}}{\rho} \\ \overline{\theta} \\ \overline{N} \end{bmatrix} \tag{39}$$

where $\psi = s^2(1 + \tau_0 s)/(s + \omega^*)$.

When Eqs. (36)–(38) are decoupled, then we get

$$\left(\nabla^6 - \alpha_2 \nabla^4 + \alpha_1 \nabla^2 - \alpha_0\right)\left\{\overline{\theta}, \overline{N}, \overline{e}\right\} = 0, \tag{40}$$

where α_2, α_1 and α_0 are specified by

$$\begin{aligned}
&\alpha_2 = s^2 + g_7 + \frac{g_6}{g_3}, \alpha_1 = s^2 g_7 + g_8 + \frac{g_6 g_5}{g_3}, \alpha_0 = s^2 g_8,\\
&g_4 = s g_1 + g_2, g_5 = g_4 - g_3, g_6 = g_3 \psi \varepsilon_1,\\
&g_7 = g_4 + \psi, g_8 = g_4 \psi + s^2 g_3 \varepsilon_2
\end{aligned} \tag{41}$$

Presenting λ_i, $(i = 1,\ 2,\ 3)$ into Eq. (40), we obtain

$$\left(\nabla^2 - \lambda_1^2\right)\left(\nabla^2 - \lambda_2^2\right)\left(\nabla^2 - \lambda_3^2\right)\left\{\overline{\theta},\ \overline{N},\ \overline{e}\right\} = 0 \tag{42}$$

where λ_1^2, λ_2^2 and λ_3^2 are the roots of the equation

$$\lambda^6 - \alpha_2 \lambda^3 + \alpha_1 \lambda^2 - \alpha_0 = 0 \tag{43}$$

which are given by

$$\begin{aligned}
\lambda_1^2 &= \frac{1}{3}\left[2\beta_0 \sin(\gamma_0) + \alpha_2\right],\\
\lambda_2^2 &= -\frac{1}{3}\beta_0\left[\sin(\gamma_0) + \sqrt{3}\cos(\gamma_0)\right] + \frac{1}{3}\alpha_2,\\
\lambda_2^2 &= \frac{1}{3}\beta_0\left[\sqrt{3}\cos(\gamma_0) - \sin(\gamma_0)\right] + \frac{1}{3}\alpha_2
\end{aligned} \tag{44}$$

with

$$\beta_0 = \sqrt{\alpha_2^2 - 3\alpha_1}, \gamma_0 = \frac{1}{3}\sin^{-1}\left(-\frac{2\alpha_2^3 - 9\alpha_2\alpha_1 + 27\alpha_0}{2\beta_0^3}\right) \tag{45}$$

The general solution to Eq. (42) can be written as

$$\left\{\overline{e},\ \overline{\theta},\ \overline{N}\right\} = \sum_{i=1}^{3}\{1,\ L_i,\ H_i\} A_i K_0(\lambda_i \rho) \tag{46}$$

where $K_{\mathrm{n}}(.)$ indicates the second type of modified Bessel functions of order n. The function $K_{\mathrm{n}}(.)$ is exponentially decaying, unlike conventional Bessel functions, which are oscillatory. The three parameters A_i, $(i = 1,\ 2,\ 3)$ are dependent on s. In addition, L_i and M_i are two distinct factors that are correlated to A_i. We get the following relations by inserting Eq. (46) into Eqs. (36)–(38)

$$H_i = \frac{g_3\left(\lambda_i^2 - s^2\right)}{\lambda_i^4 - g_5 \lambda_i^2}, \quad L_n = \frac{\left(\lambda_i^2 - s^2\right)\left(\lambda_i^2 - g_4\right)}{\lambda_i^4 - g_5 \lambda_i^2}, \quad i = 1,\ 2,\ 3 \tag{47}$$

The cubical dilatation e in the Laplace transform domain is expressed as

$$\overline{e} = \frac{1}{\rho}\frac{\partial}{\partial \rho}(\rho \overline{u}) = \sum_{i=1}^{3} A_i K_0(\lambda_i \overline{\rho}) \tag{48}$$

When both sides of the above equation are integrated with regard to ρ, we obtain

$$\overline{u} = -\sum_{i=1}^{3}\frac{1}{m_i} A_i K_1(\lambda_i \rho) \tag{49}$$

Equation (49) is differentiated in terms of ρ to provide

$$\frac{\mathrm{d}\overline{u}}{\mathrm{d}\rho} = \sum_{i=1}^{3} A_i\left(K_0(\lambda_i \rho) + \frac{1}{\rho \lambda_i} K_1(\lambda_i \rho)\right) \tag{50}$$

Consequently, the closed form solutions for thermal stresses are as follows:

$$\begin{aligned}
\overline{\sigma}_{\rho\rho} &= \sum_{i=1}^{3} A_i \left(\Omega_i K_0(\lambda_i \rho) + \frac{2\beta^2}{\rho\lambda_i} K_1(\lambda_i \rho) \right), \\
\overline{\sigma}_{\phi\phi} &= \sum_{i=1}^{3} A_i \left(\Phi_i K_0(\lambda_i \rho) + \frac{2\beta^2}{\rho\lambda_i} K_1(\lambda_i \rho) \right), \\
\overline{\sigma}_{zz} &= \sum_{i=1}^{3} A_i \Phi_i K_0(\lambda_i \rho)
\end{aligned} \tag{51}$$

where

$$\Omega_i = 1 - L_i - H_i, \quad \Phi_i = 1 - 2\beta^2 - L_i - H_i \tag{52}$$

The non-dimensional Maxwell's stress $\overline{\tau}_{\rho\rho}$ is given by

$$\overline{\tau}_{\rho\rho} = \frac{v_a^2}{v_0^2} e = \frac{v_a^2}{v_0^2} \sum_{i=1}^{3} A_i K_0(\lambda_i \rho) \tag{53}$$

The boundary conditions (30), (33) and (34) have the following forms after performing the Laplace transform:

$$\begin{gathered}
\left.\frac{\partial \overline{\theta}}{\partial \rho}\right|_{\rho=\rho_0} = -\frac{s q_0 (1+s\mathrm{t}0)\mathrm{tp}^3}{8 t_p^2 (s+\omega^*)(1+s\mathrm{tp})^3} = -\overline{G}(s), \\
\overline{\sigma}_{\rho\rho}(\rho_0, \mathrm{s}) = 0, \\
D_E \left.\frac{\partial \overline{N}}{\partial \rho}\right|_{\rho=\rho_0} = s_f \overline{N}(\rho_0, s)
\end{gathered} \tag{54}$$

Equations (46) and (51) are substituted into Eq. (54), giving

$$\begin{aligned}
&\sum_{i=1}^{3} \lambda_i A_i K_1(\rho_0 \lambda_i) = \overline{G}(s), \\
&\sum_{i=1}^{3} \frac{1}{m_i} A_i K_1(\rho_0 \lambda_i) = 0, \\
&\sum_{i=1}^{3} A_i H_i \left((D_E - s_v) K_0(\lambda_i \rho_0) + \frac{D_E}{\rho_0 \lambda_i} K_1(\lambda_i \rho_0) \right) = 0
\end{aligned} \tag{55}$$

We derive the values of the parameters A_i, $(i = 1,\ 2,\ 3)$ by solving the system (55).

The inversion of Laplace transforms was obtained in this study using an accurate and efficient numerical approach based on Fourier series expansion [48]. Any function in the Laplace domain can be inverted to the time domain using this method as follows:

$$\Gamma(\rho, t) = \frac{e^{ct}}{t} \left(\frac{1}{2} \overline{\Gamma}(\rho, c) + \mathrm{Re} \sum_{j=1}^{N_f} \overline{\Gamma}\left(\rho, c + \frac{ij\pi}{t} \right) (-1)^j \right) \tag{56}$$

where N_f denotes the number of terms, Re denotes the real part, and i denotes the imaginary number unit. Numerous numerical tests have demonstrated that the value of the parameter c fulfills the relation $c\tau \cong 4.7$, allowing for quicker convergence [49].

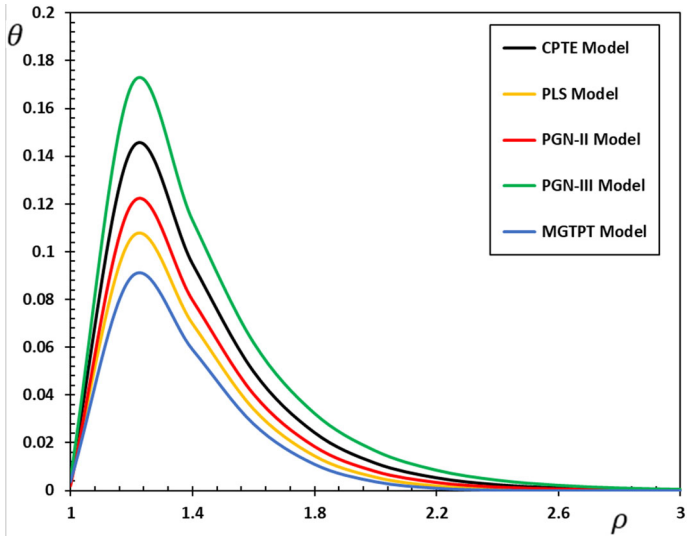

Fig. 1 The temperature variation θ for different models of photo-thermoelasticity

5 Numerical results

To demonstrate the theoretical results obtained in the previous sections, we will now present some numerical findings. Using Mathematica software, the influence of the modified photothermal heat equation (MGTPT), which is defined by the Moore-Gibson-Thompson (MGT) equation, on the studied physical fields can now be seen as graphical representations and tables. In the theoretical analysis, isotropic silicon (Si) is used as the semiconductor solid material in the device. The physical parameters utilized at $T_0 = 300$ K are as follows [26]:

$$\begin{aligned}
&\lambda = 3.64 \times 10^{10}\,\mathrm{kg\,m^{-1}s^{-2}},\ \mu = 5.46 \times 10^{10}\,\mathrm{kg\,m^{-1}s^{-2}},\ \rho = 2330\,\mathrm{kg\,m^{-3}},\\
&K = 1.51\,\mathrm{Wm^{-1}K^{-1}},\ C_E = 6.95 \times 10^2\,\mathrm{JkgK^{-1}},\ d_n = -9 \times 10^{-31}\,\mathrm{m^3},\\
&E_g = 1.11\,\mathrm{eV},\ D_E = 2.5 \times 10^{-3}\,\mathrm{m^2s^{-1}},\ s_f = 2\,\mathrm{ms^{-1}},\ \tau = 5 \times 10^{-5}\,\mathrm{s}
\end{aligned}$$

In the context of the coupled theory of thermal-plasma-elastic waves under the MGTE model, the numerical approach described in (56) has been used to distribute the distribution of non-dimensional temperature θ, the radial displacement u, the radial and hoop stresses $\sigma_{\rho\rho}$ and $\sigma_{\phi\phi}$, Maxwell's stress $\tau_{\rho\rho}$ and the absolute carrier density N along the radial direction of the cylinder. Figures 1, 2, 3, 4, 5, 6, 7, 8, 9, 10 and 11 graphically depict the numerical findings for time $t = 0.12$s and $\rho_0 = 1$.

5.1 Verification of the results

To validate the numerical results and the validity of the proposed MGTPT photo-thermoelastic model, a numerical comparison with the results of Abbas and Aly [50], Lotfy et al. [51] and Khamis et al. [52] and Abouelregal [53] was done. The governing equations in [51–53] were applied using the Lord and Shulman [2], Green—Naghdi [4], and Green and Lindsay [3] photo-thermoelastic models, whereas the current model introduced and applied the Moore-Gibson-Thompson photo-thermoelastic model (MGTPT) [43]. By comparing the results, it was discovered that the thermal parameters τ_0 and K^* of the photothermal model (MGTPT) have a significant influence on the studied fields, despite the agreement in behavior and convergence in numerical values. In addition, the presence of the thermal parameters τ_0 in the proposed model reduces and relaxes the mechanical and thermal wave behavior.

In three additional cases, numerical calculations will be performed for all studied field variables.

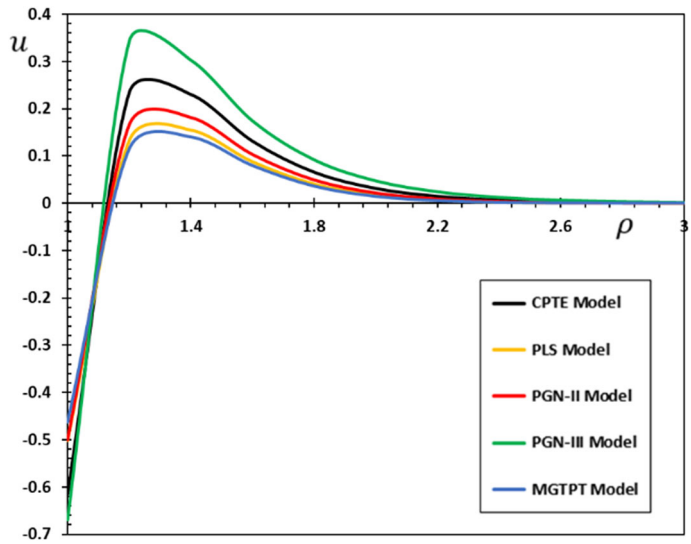

Fig. 2 The displacement variation u for different models of photo-thermoelasticity

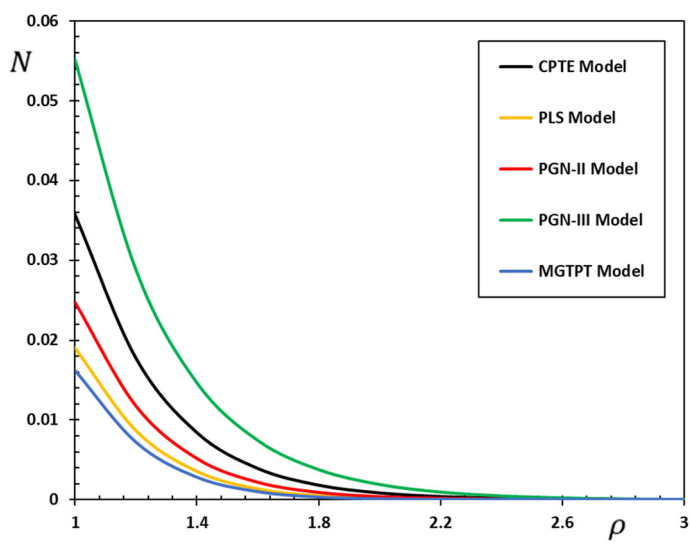

Fig. 3 The carrier density N variation for different models of photo-thermoelasticity

5.2 Comparison of several thermoelasticity models

The suggested Moore-Gibson-Thompson photothermal (MGTPT) model is a generalization of several photo-thermoelasticity models used in this study. It was provided not only to generalize but also to solve some of the physical consequences found in some earlier models. In the first and second sections, many inconsistencies are addressed.

Many earlier models of photo-thermoelasticity can be derived as special instances by reference to the modified Moore–Gibson–Thompson heat conduction equation (MGTPT). When $\tau_0 = K^* = 0$, the coupled photo-thermoelasticity theory (CPTE) is obtained, and when $K^* = 0$, the generalized Lord and Shulman photo-thermoelasticity model (PLS) is obtained. Furthermore, the photothermal Green and Naghdi model (PGN-III) can be obtained if the relaxation parameter $\tau_0 = 0$ is omitted, and the photothermal Green and Naghdi model (PGN-II) may be obtained if the term that contains the parameter K is absent. If $\tau_0, K^* > 0$, this indicates that the photothermal model (MGTPT) is used.

The present subsection will examine the comparison of the newly given model with other previous photothermal models in order to verify them. To illustrate comparison and research, as well as for practical

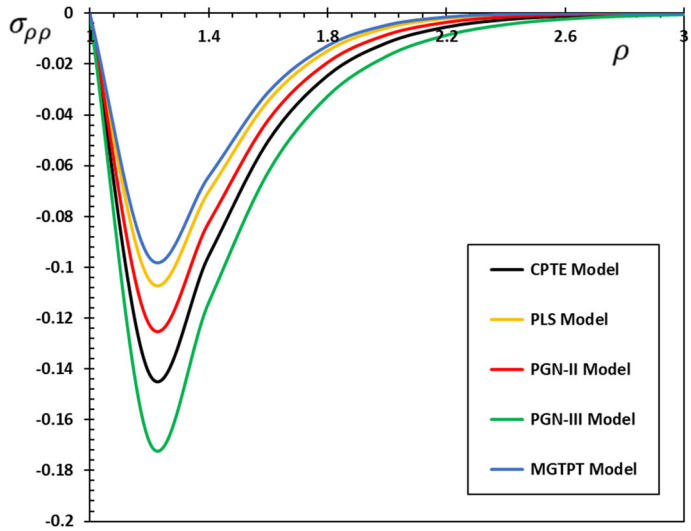

Fig. 4 The radial stress variation $\sigma_{\rho\rho}$ for different models of photo-thermoelasticity

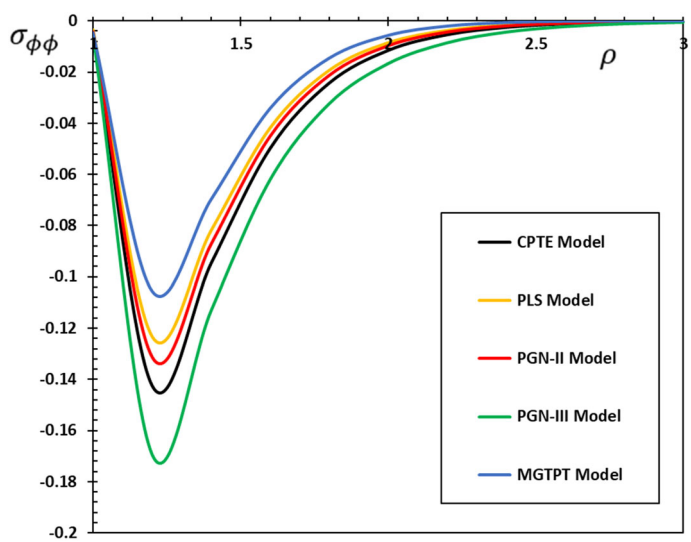

Fig. 5 The hoop stress variation $\sigma_{\phi\phi}$ for different models of photo-thermoelasticity

purposes, tables and figures will be used to illustrate discussions and comparisons. Tables 1, 2, 3, 4, 5 and 6 as well as Figs. 1, 2, 3, 4, 5 and 6 show the changes in investigated studied fields against radial distance ρ for the CPTE, PLS, PGN-II, PGN-III, and MGTPT models. In this case, the non-dimensional carrier lifetime parameter τ and the pulsing heat flux duration time t_p are fixed ($\tau = 0.01,\ t_p = 0.15$).

The change of the absolute value of non-dimensional temperature θ with regard to radial distance ρ is shown in Fig. 1. It has been discovered that as ρ increases, the temperature θ values increase until they reach a maximum around $\rho = 1.2$, after which they decrease monotonically with increasing distance ρ. The magnitudes of carrier density N as a function of distance ρ are depicted in Fig. 2. The graphic shows that the carrier density N value is highest near the surface and subsequently declines in a monotonous manner as the distance from the cavity increases. Figure 3 shows how the radial displacement u varies with distance ρ. The displacement grows rapidly with increasing r until it reaches the peak point, after which it decreases monotonically from the boundary surface away from the application of the laser pulse heat flux.

Figures 4 and 5 illustrate the radial and hoop stresses $\sigma_{\rho\rho}$ and $\sigma_{\phi\phi}$, in photo-thermoelastic media for various photothermal models with regard to radius ρ for different models of photothermal. The radial pressure $\sigma_{\rho\rho}$ on the cavity surface ($\rho = 1$) is zero in all representations, which corresponds to the case of the mechanical boundary of the problem where the cavity surface is free of traction. From the figures, it can be observed that

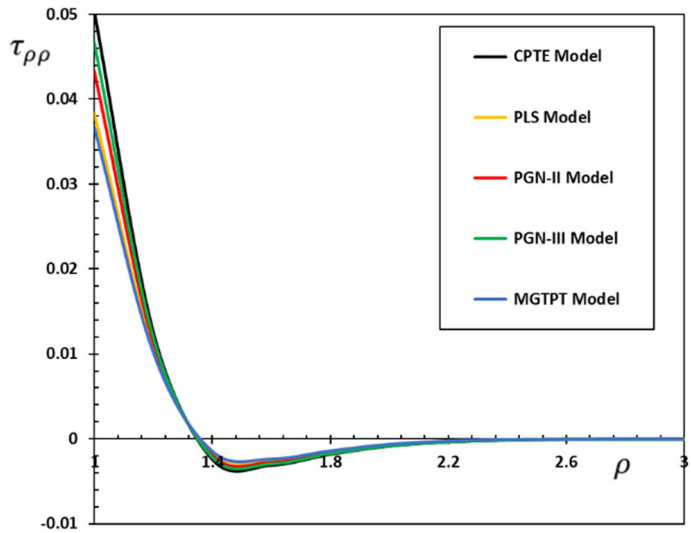

Fig. 6 The Maxwell's stress $\tau_{\rho\rho}$ for different models of photo-thermoelasticity

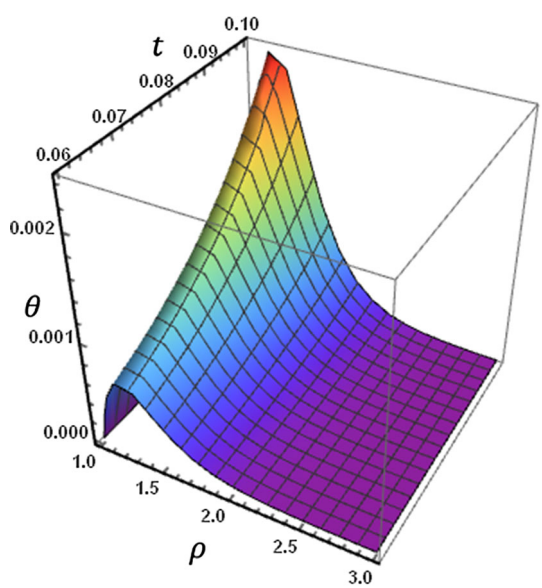

Fig. 7 The 3D plot of the temperature θ versus the distance ρ and instant time t

Table 1 The variation of the temperature θ against the radial distance ρ

r	CPTE	PLS	PGN-II	PGN-III	MGTPT
1	0.00448047	0.00451887	0.00180564	0.00522654	0.00375518
1.2	0.14278600	0.10578100	0.11973100	0.16954400	0.08934000
1.4	0.09504820	0.06999120	0.07970440	0.11335100	0.05906150
1.6	0.04998960	0.03434300	0.04039950	0.06217240	0.02802530
1.8	0.02439680	0.01469320	0.01841330	0.03248600	0.01111790
2	0.01157230	0.00574802	0.00794450	0.01677240	0.00379131
2.2	0.00543004	0.00209105	0.00331837	0.00864885	0.00107774
2.4	0.00253927	0.000709288	0.00135766	0.00446829	0.000218371
2.6	0.00118721	0.000222315	0.000547798	0.00231448	0.0000008982
2.8	0.000555702	0.0000626562	0.000218910	0.00120195	0.000029955
3	0.000260532	0.0000147247	0.0000868866	0.000625658	0.0000209335

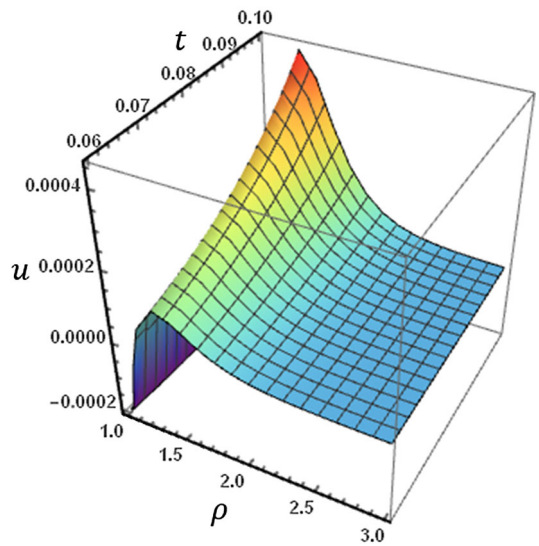

Fig. 8 The 3D plot of the displacement u versus the radial distance ρ and instant time t

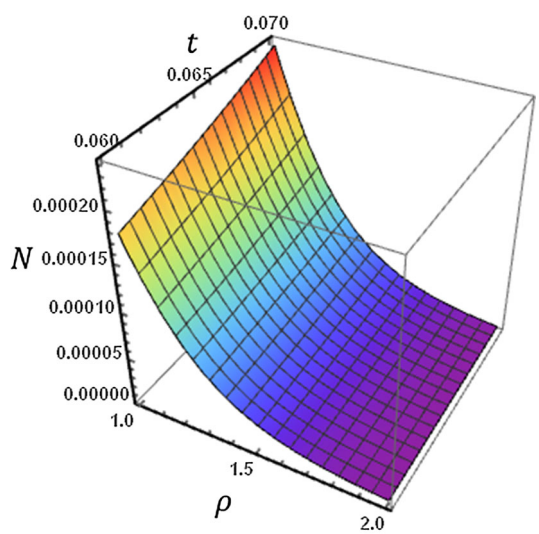

Fig. 9 The 3D plot of the carrier density N versus the distance ρ and instant time t

Table 2 The variation of the displacement u against the radial distance ρ

r	CPTE	PLS	PGN-II	PGN-III	MGTPT
1	− 0.6146860	− 0.5020980	− 0.500120	− 0.669967	− 0.4627400
1.2	0.2340620	0.13298100	0.1665100	0.3428190	0.11486500
1.4	0.2302130	0.15477300	0.1819500	0.3030590	0.13974900
1.6	0.1313330	0.08776720	0.1035590	0.1743630	0.07926850
1.8	0.0657977	0.04045710	0.0496004	0.0918823	0.03578150
2	0.0314727	0.01667140	0.0219710	0.0473547	0.01410010
2.2	0.0147895	0.00634001	0.0093214	0.0243125	0.00496429
2.4	0.0069069	0.00224874	0.00385147	0.0125019	0.00154802
2.6	0.00322162	0.000742812	0.00156410	0.00644753	0.000406303
2.8	0.00150395	0.000225318	0.000627759	0.00333529	7.34597E − 05
3	0.000703257	6.04179E − 05	0.00024989	0.00173018	− 3.85393E − 06

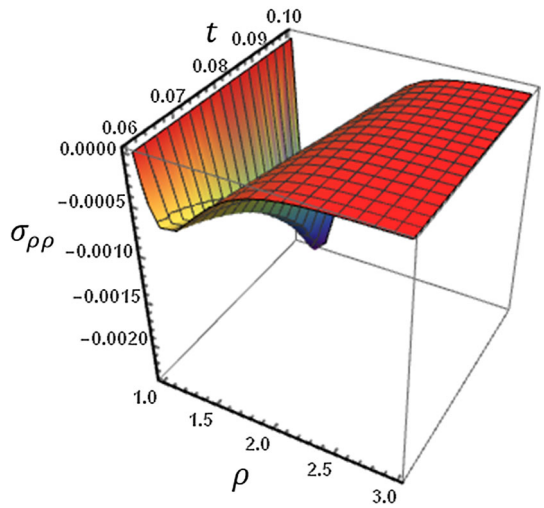

Fig. 10 The 3D plot of the radial stress $\sigma_{\rho\rho}$ versus the radial distance ρ and instant time t

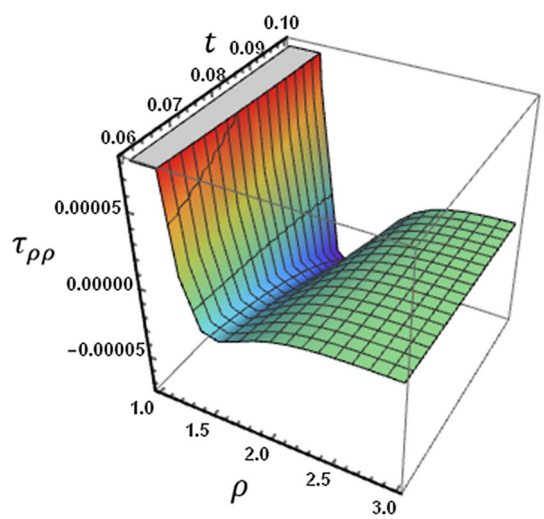

Fig. 11 The 3D plot of the Maxwell stress $\tau_{\rho\rho}$ versus the radial distance ρ and instant time t

Table 3 The variation of the carrier density N against the radial distance ρ

r	CPTE	PLS	PGN-II	PGN-III	MGTPT
1	0.0357853	0.0190579	0.0248371	0.0551856	0.0162936
1.2	0.0177977	0.00867268	0.0117863	0.0288679	0.00724007
1.4	0.00842566	0.00353148	0.00516636	0.0147179	0.00281451
1.6	0.00392045	0.00132969	0.00217099	0.00748081	0.000980057
1.8	0.00181508	0.000467862	0.00088956	0.00381402	0.000303018
2	0.000840325	0.000153596	0.000358658	0.00195301	7.90951E − 05
2.2	0.000389796	4.63963E − 05	0.000143052	0.00100427	1.43309E − 05
2.4	0.000181278	1.24252E − 05	5.66357E − 05	0.000518345	6.42611E − 07
2.6	8.45286E − 05	2.64393E − 06	2.23069E − 05	0.000268404	2.36229E − 06
2.8	3.95143E − 05	2.31013E − 07	8.75416E − 06	0.000139371	− 1.55019E − 06
3	0.000018514	− 1.8205E − 07	3.42681E − 06	7.25449E − 05	7.5685E − 07

Table 4 The variation of the radial stress $\sigma_{\rho\rho}$ against the radial distance ρ

r	CPTE	PLS	PGN-II	PGN-III	MGTPT
1	0	0	0	0	0
1.2	− 0.141744	− 0.104855	− 0.122523	− 0.168542	− 0.0961487
1.4	− 0.0955306	− 0.0702822	− 0.0825105	− 0.114022	− 0.0644194
1.6	− 0.0504102	− 0.034645	− 0.0421969	− 0.0627014	− 0.0312148
1.8	− 0.0246317	− 0.0148613	− 0.0194658	− 0.0327842	− 0.0128925
2	− 0.0116891	− 0.00582494	− 0.00853475	− 0.0169285	− 0.00473107
2.2	− 0.00548574	− 0.00212263	− 0.00363764	− 0.00872909	− 0.00154639
2.4	− 0.0025654	− 0.000721265	− 0.00152463	− 0.00450942	− 0.00043611
2.6	− 0.00119941	− 0.000226554	− 0.000632491	− 0.00233561	− 9.43055E − 05
2.8	− 0.000561388	− 6.40532E − 05	− 0.000260737	− 0.00121283	− 6.60157E − 06
3	− 0.000263185	− 1.51472E − 05	− 0.000107074	− 0.000631285	8.18E − 06

Table 5 The variation of the hoop stress $\sigma_{\phi\phi}$ against the radial distance ρ

r	CPTE	PLS	PGN-II	PGN-III	MGTPT
1	− 0.00478359	− 0.00332681	− 0.00419168	− 0.00553329	− 0.0047073
1.2	− 0.14252000	− 0.12331600	− 0.1312200	− 0.16919100	− 0.1056070
1.4	− 0.09491780	− 0.08202640	− 0.0872858	− 0.11318200	− 0.0699013
1.6	− 0.04993690	− 0.04179800	− 0.04506020	− 0.06210040	− 0.0343092
1.8	− 0.02437660	− 0.01925210	− 0.02126930	− 0.03245570	− 0.0146824
2	− 0.01156470	− 0.00843472	− 0.00964625	− 0.01675960	− 0.00574502
2.2	− 0.00542718	− 0.00359359	− 0.00429110	− 0.00864338	− 0.00209036
2.4	− 0.00253820	− 0.00150586	− 0.00189098	− 0.00446594	− 0.000709181
2.6	− 0.00118682	− 0.000624643	− 0.000829725	− 0.00231347	− 0.000222323
2.8	− 0.000555559	− 0.000257493	− 0.000363486	− 0.00120151	− 6.26723E − 05
3	− 0.000260481	− 0.000105742	− 0.000159212	− 0.000625471	− 1.47338E − 05

Table 6 The Maxwell's stress $\tau_{\rho\rho}$ against the radial distance ρ

r	CPTE	PLS	PGN-II	PGN-III	MGTPT
1	0.05044140	0.038384300	0.043292900	0.046664200	0.03676470
1.2	0.01261400	0.010559800	0.011456200	0.012023400	0.01024540
1.4	− 0.00240053	− 0.00155058	− 0.001875520	− 0.002114730	− 0.00144903
1.6	− 0.00311251	− 0.00245645	− 0.002721710	− 0.002904560	− 0.00236856
1.8	− 0.00182249	− 0.00145528	− 0.00160320	− 0.001705530	− 0.00140633
2	− 0.000863584	− 0.000654316	− 0.000736636	− 0.000795198	− 0.000627722
2.2	− 0.000367158	− 0.000245808	− 0.000292332	− 0.000326449	− 0.000231201
2.4	− 0.000145199	− 7.72107E − 05	− 0.000102623	− 0.000121815	− 6.94535E − 05
2.6	− 5.42248E − 05	− 1.85111E − 05	− 3.14581E − 05	− 4.15781E − 05	− 1.46865E − 05
2.8	− 1.92289E − 05	− 1.81614E − 06	− 7.86372E − 06	− 1.28196E − 05	− 1.10104E − 07
3	− 6.46954E − 06	1.39239E − 06	− 1.16829E − 06	− 3.41784E − 06	2.06376E − 06

thermal stresses are usually compressive. In Fig. 6, the change in Maxwell stress $\tau_{\rho\rho}$ in relation to distance ρ was displayed. Figure 2 shows that the Maxwell stress $\tau_{\rho\rho}$ variance takes its highest surface value and declines rapidly until reaching its lowest point, then grows extremely monotonously until it disappears.

In addition to the previous observations from Tables 1, 2, 3, 4, 5 and 6, we can mention some noteworthy facts.

- The existence of variations in the fields is obviously developing over time in the photothermal MGTPT model and has an important influence across all domain profiles examined.
- The thermal parameters τ_0 and K^* has a significant impact on all of the domains investigated, as seen in the graphs.
- The phenomena of restricted thermal transmission velocity of the photo-thermoelasticity MGTPT theory is well understood in all Figures and Tables.
- Different domain distributions have a limited prevalence. This is in contrast to cases where coupling and decoupling theorems in photo-thermoelasticity have an infinite propagation rate, which results in nonzero values for all functions anywhere in the medium.

- The coupled photothermal model (CPTE), as well as modified and generalized photothermal models (PLS, PGNII, PGNIII, and MGTPT), give values that are different in magnitude but similar in behavior at the surface of the semiconducting cylinder, where the boundary conditions appear.
- For all physical domains, all curves converge, where ρ tends to zero to meet the regularity requirement.
- The temperature of GN-III is likewise found to be higher than that of MGTE, with comparable results for the PLS and MGTPT models.
- The results of the frequently used GN-III thermal elasticity model show that it varies considerably from the GN-II thermal elasticity models in terms of reduced energy dissipation.
- In the LS and MGTE models, the inclusion of the relaxation parameter might result in a slower temperature decline.
- The solution instantly fills the entire medium in the case of the CPTE coupled and the PGNIII model. The solution is thus not the same zero for every tiny value of time (although it may be very small). The solution achieved with the MGTPT photo-thermoelasticity model equations, however, shows the comportment of final wave propagation velocities.
- The PGN-III results also show convergence from the conventional elasticity model (CPTE), which, unlike other generalized thermoelasticity models, does not vanish quickly inside the body due to heat. This is fully consistent with Quintanilla's claims [14] and Abouelregal et al. observations [17–19].
- In one section of the cylinder, all kinds of pressure are compressed, while in another area, there is tension. Tensile highlights that the medium next to the cylinder surface is positioned throughout time, and this conforms to the information given in [54]. Furthermore, the higher value and amplitude of fields measured at the cavity surface are obvious with the rise in radial breadth. The explanations for this occurrence are included in [55].
- For small time values, the solution is located in a limited area of space enclosing the spherical cavity, and beyond this region is identically null. The area becomes longer and fills up the middle of the medium. The boundary of the wavefront is located. All models provide almost identical findings for long time values. This is because the second sound effects are not long enough.

5.3 The effect of the instant time

For constant values of carrier lifetime τ and laser pulse duration t_p parameters, Figs. 7, 8, 9, 10 and 11 depict changes in the behavior of photothermal field variables as functions of distance ρ and time t in 3D plots. In this case, the discussion was carried out in the context of the proposed model of photo-thermoelasticity (MGTPT), which includes relaxation time. Figures 7, 8, and 9 show that as time t passes, the carrier density N, temperature θ, and the amount of displacement u distributions increase along the radial direction. Figures 10 and 11 demonstrate the change of radial stress $\sigma_{\rho\rho}$ and Maxwell stress $\tau_{\rho\rho}$ against the radial distance ρ over the instant time t. It was discovered that when the values of time along the ρ-direction grow, the distributions decrease.

All of these diagrams demonstrate the phenomena of limited propagation speeds. The photothermal impacts of the surrounding medium are confined to an area near the cavity for the smallest values of time taken into account. For the maximum value of time, this area grows to fill the whole medium. The propagation of wavefronts from the cavity of an unbounded medium is shown in this region. The classical coupled photothermal theory (CPTE), on the other hand, does not have this problem since thermal impacts are instantly felt throughout the medium.

Due to laser pulse heat flux, the medium attached to the cylindrical cavity surface is expanded, and the others are compressively deformed. Deformation is a process that is dynamic. Over time, the growth zone is progressively moving inside and getting bigger and bigger. The displacement u is, therefore, increasing and growing. At a given moment, the nonzero radial area is limited owing to the thermal-and plasma-based wave effect. It implies that photothermal transfers with a limited velocity over time into the depth of the material. The more instantly the thermal area and the displacement are evaluated, the more appropriate.

The medium at the cavity surface is subject to a tensile stress that increases with time. The presence of stress at the cavity surface could be attributed to the effects of cross-effects caused by the connection of the temperature, photothermal, and strain fields. Due to these intersectional effects, the laser excitation leads to the generation of a further photothermal field of thermal stress.

Table 7 Effects of carrier lifetime and laser pulse duration parameters on the dimensionless physical fields

τ	t_p	Photothermal physical fields				
		θ	N	u	$\sigma_{\rho\rho}$	$\tau_{\rho\rho}$
0.0010	0.10	0.1096020	0.00936350	0.0141481	− 0.1086590	0.01261400
	0.11	0.0952248	0.00813520	0.0122921	− 0.0944050	0.01095930
	0.12	0.0834737	0.00713128	0.0107752	− 0.0827550	0.00960688
	0.13	0.0737530	0.00630083	0.00952045	− 0.0731181	0.00848815
0.0012	0.10	0.1175260	0.0212263	0.0211393	− 0.1167550	0.01118950
	0.11	0.1021090	0.0184418	0.0183663	− 0.1014390	0.00972166
	0.12	0.0895079	0.0161660	0.0160998	− 0.0889212	0.00852197
	0.13	0.0790846	0.0142835	0.0142250	− 0.0785662	0.00752957
0.0013	0.10	0.1203870	0.0302383	0.0272163	− 0.119772	0.00990401
	0.11	0.1045950	0.0262717	0.0236460	− 0.104060	0.00860480
	0.12	0.0916876	0.0230297	0.0207280	− 0.0912185	0.00754294
	0.13	0.0810104	0.0203478	0.0183142	− 0.0805960	0.00666455
0.0014	0.10	0.122520	0.0428456	0.035965	− 0.122125	0.00806922
	0.11	0.106448	0.0372251	0.0312471	− 0.106105	0.0070107
	0.12	0.0933118	0.0326314	0.0273911	− 0.0930111	0.00614556
	0.13	0.0824455	0.0288314	0.0242013	− 0.0821798	0.0054299

5.4 The effect of carrier lifetime and laser pulse duration parameters

Exploration of lasers was useful to understand the properties of a material's inner structure, and as a result, various modern applications in physical sciences, engineering, and medicine have emerged. The thermal effect of a non-Gaussian laser on a thermoelastic material that is employed as a heat source is highly relevant under the influence of extended thermoelastic theories.

The use of photothermal excitation of shorter elastic pulses (high-frequency elastic waves) in various fields of practical physics is now of great interest. When a laser beam (laser light source) was incident on an intracavity sample, the laser pulses caused the temperature to increase. The free carrier's chargeintensity appears after all excited electrons have been photo-excited. The fact that photothermal-produced ultrasonic waves contain information about the producing medium and surrounding media has enabled the creation of one-dimensional theoretical models.

Theoretical and practical ways of obtaining information on carrier intrinsic concentrations and a long carrier lifetime τ are critical criteria for modeling semiconductor devices in order to comprehend and improve device physics and performance. The minority carrier movement and effective carrier lifetime parameter τ of the absorber material for solar cells affect the open-circuit voltage and photo-generated current density N in particular.

The phenomena of microwave heating using pulsed lasers is investigated in this section. The solid cylinder is constructed of silicon and heated by a pulsed non-Gaussian laser beam with a duration of t_p, causing the vibration to be dampened by thermoelasticity. Energy dissipation occurs when temperature and stress combine, turning mechanical energy into permanent heat energy. Table 7 shows how the duration of a laser pulse t_p and the lifespan parameter τ, influence the dimensionless thermo-physical investigated fields at $\rho = 1.1$. The study in this subsection will be carried out in light of Moore-Gibson-Thomson's photo-thermoelastic modified theory (MGTPT).

The investigated fields, comprising temperature, displacement carrier density, and thermal stress components, are dependent not only on distance ρ and time t but also on the duration of the laser pulse t_p and the photo-generated carrier lifespan parameter τ, as shown in Table 7. Moreover, thermal and mechanical waves are more sensitive to the change of laser duration t_p than to the change of lifetime τ.

The values of the temperature θ, carrier density N, and radial displacement u have all been demonstrated to decrease as the time of the laser pulse t_p grows, but the values of thermal stress $\sigma_{\rho\rho}$ and Maxwell's stress $\tau_{\rho\rho}$ have both increased. From the Table, it can be seen that by increasing the photo-generated carrier lifetime parameter τ, we find that there is an increase in the temperature, carrier density N, the magnitudes of the thermal stress $\sigma_{\rho\rho}$ and Maxwell's stress $\tau_{\rho\rho}$. However, the radial displacement u distribution decreases with the increase in value of the lifetime parameter τ.

In the investigation of the macroscopic output of some materials pertaining to photothermal materials, which dominate in the determination of material characteristics, the carrier lifetime parameter τ will play a

significant role. All of these findings demonstrate the concept of limited heat dispersion rates. For designers of novel materials and other disciplines of materials science and physical engineering, the results obtained in this example might be useful in the presence of plasma waves and elasticity. Because of flaws and a lack of information about material characteristics, measuring carrier lifetime in many thin-film photovoltaic materials may be challenging.

Rapidly varying contraction and expansion cause temperature fluctuations in materials susceptible to heat transmission by conduction [56]. Because pulsed laser technologies are widely utilized in material processing, nondestructive testing, and characterization, this mechanism has attracted a lot of attention [57].

6 Conclusion

This study offers a new photothermoelastic model of heat conduction based on the Moore-Gibson-Thompson equation. The improved photothermal model includes the Type III Green-Naghdi model, as well as the Lord and Shulman heat transfer equation. This expanded model is used to explore the interaction of heat, plasma, and elastic waves in semiconducting materials. Only a few reviews of the literature on our model have been published due to the complexity of the governing equations in extended photothermal theory. As special instances, many thermoelastic and photothermal models may be developed from a given model.

According to the discussions, the following important conclusions can be summarized:

- Thermal parameters have a major influence on the distributions of photothermal field values. In the fields studied, the effects of laser pulse duration and lifetime characteristics are also important.
- The temperature passes through the medium as a finite velocity wave in the new stretched thermal image-flexible MGTPT model rather than as an infinite velocity wave in the classical models. Thus, the generalized MGTPT model can be considered better in understanding the photo-thermoelastic process than the PGN-III model. Coupled photo-thermoelastic and generalized models provide close results for high time values. On the contrary, when we examine the short value of time, the situation is quite different.
- Due to the laser pulsed heat flow, the medium attached to the surface of the cylindrical cavity is expanded, and the cylinder is compactly deformed.
- When comparing the solutions, it can be concluded that the lifespan coefficient is an important phenomenon and has a great influence on the distribution of different physical domains.

The proposed work in this study is a theoretical basis for describing the photoacoustic effect in semiconductors that takes into account the thermal effects, diffusion, and recombination of carriers. The ideas presented in this study can also be very useful to scientists working in areas such as physics, material design, thermal efficiency, and geophysics. Finally, the method used in the present work can be used to address a variety of thermoelastic and thermodynamic problems.

Acknowledgements The authors would like to acknowledge the Deanship of Scientific Research at Jouf University for funding this work through research Grant No. (DSR-2021-03-03177). We would also like to extend our sincere thanks to the College of Science and Arts in Al-Qurayyat for their support.

Author contributions All authors discussed the results, reviewed and approved the final version of the manuscript.

Declarations

Conflict of interest The author(s) declared no potential conflicts of interest with respect to the research, authorship and publication of this article.

References

1. Biot, M.A.: Thermoelasticity and irreversible thermodynamics. J. Appl. Phys. **27**, 240–253 (1956)
2. Lord, H.W., Shulman, Y.: A generalized dynamical theory of thermoelasticity. J. Mech. Phys. Solids **15**(5), 299–309 (1967)
3. Green, A.E., Lindsay, K.A.: Thermoelasticity. J. Elast. **2**(1), 1–7 (1972)
4. Green, A.E., Naghdi, P.M.: A re-examination of the basic postulates of thermomechanics. Proc. R. Soc. A Math. Phys. Eng. Sci. **432**, 171–194 (1991)
5. Green, A.E., Naghdi, P.M.: On undamped heat waves in an elastic solid. J. Therm. Stress. **15**(2), 253–264 (1992)
6. Green, A.E., Naghdi, P.M.: Thermoelasticity without energy dissipation. J. Elast. **31**(3), 189–208 (1993)

7. Abouelregal, A.E.: Modified fractional thermoelasticity model with multi-relaxation times of higher order: application to spherical cavity exposed to a harmonic varying heat. Waves Random Complex Media (2019). https://doi.org/10.1080/17455030.2019.1628320
8. Abouelregal, A.E.: Two-temperature thermoelastic model without energy dissipation including higher order time-derivatives and two phase-lags. Mater. Res. Express **6**(11), 116535 (2019)
9. Abouelregal, A.E.: On Green and Naghdi thermoelasticity model without energy dissipation with higher order time differential and phase-lags. J. Appl. Comput. Mech. **6**(3), 445–456 (2020)
10. Abouelregal, A.E.: A novel generalized thermoelasticity with higher-order time-derivatives and three-phase lags. Multidiscip. Model. Mater. Struct. **16**(4), 689–711 (2019)
11. Abouelregal, A.E.: Three-phase-lag thermoelastic heat conduction model with higher-order time-fractional derivatives. Indian J. Phys. **94**, 1949–1963 (2020)
12. Abouelregal, A.E., Elhagary, M.A., Soleiman, A., Khalil, K.M.: Generalized thermoelastic-diffusion model with higher-order fractional time-derivatives and four-phase-lags. Mech. Based Des. Struct. Mach. (2020). https://doi.org/10.1080/15397734.2020.1730189
13. Lasiecka, I., Wang, X.: Moore–Gibson–Thompson equation with memory, part II: general decay of energy. J. Diff. Equ. **259**, 7610–7635 (2015)
14. Quintanilla, R.: Moore-Gibson-Thompson thermoelasticity. Math. Mech. Solids **24**, 4020–4031 (2019)
15. Quintanilla, R.: Moore-Gibson-Thompson thermoelasticity with two temperatures. Appl. Eng. Sci. **1**, 100006 (2020)
16. Abouelregal, A.E., Ahmed, I.-E., Nasr, M.E., Khalil, K.M., Zakria, A., Mohammed, F.A.: Thermoelastic processes by a continuous heat source line in an infinite solid via Moore–Gibson–Thompson thermoelasticity. Materials **13**(19), 4463 (2020)
17. Abouelregal, A.E., Ahmad, H., Nofal, T.A., Abu-Zinadah, H.: Moore–Gibson–Thompson thermoelasticity model with temperature-dependent properties for thermo-viscoelastic orthotropic solid cylinder of infinite length under a temperature pulse. Phys. Scr. (2021). https://doi.org/10.1088/1402-4896/abfd63
18. Aboueregal, A.E., Sedighi, H.M.: The effect of variable properties and rotation in a visco-thermoelastic orthotropic annular cylinder under the Moore Gibson Thompson heat conduction model. Proc. Inst. Mech. Eng. Part L J. Mater. Des. Appl. **235**(5), 1004–1020 (2021)
19. Aboueregal, A.E., Sedighi, H.M., Shirazi, A.H., Malikan, M., Eremeyev, V.A.: Computational analysis of an infinite magneto-thermoelastic solid periodically dispersed with varying heat flow based on non-local Moore–Gibson–Thompson approach. Contin. Mech. Thermodyn. (2021). https://doi.org/10.1007/s00161-021-00998-1
20. Abouelregal, A.E., Ersoy, H., Civalek, Ö.: Solution of Moore–Gibson–Thompson equation of an unbounded medium with a cylindrical hole. Mathematics **9**(13), 1536 (2021)
21. Kaltenbacher, B., Lasiecka, I., Marchand, R.: Wellposedness and exponential decay rates for the Moore–Gibson–Thompson equation arising in high intensity ultrasound. Control Cybern. **40**, 971–988 (2011)
22. Bazarra, N., Fernández, J.R., Quintanilla, R.: Analysis of a Moore-Gibson-Thompson thermoelastic problem. J. Comput. Appl. Math. **382**(15), 113058 (2021)
23. Lotfy, K.: The elastic wave motions for a photothermal medium of a dual-phase-lag model with an internal heat source and gravitational field. Can. J. Phys. **94**, 400–409 (2016)
24. Gordon, J.P., Leite, R.C.C., Moore, R.S., et al.: Long- transient effects in lasers with inserted liquid samples. Bull. Am. Phys. Soc. **119**, 501 (1964)
25. Todorovic, D.M., Nikolic, P.M., Bojicic, A.I.: Photoacoustic frequency transmission technique: electronic deformation mechanism in semiconductors. J. Appl. Phys. **85**, 7716 (1999)
26. Song, Y.Q., Todorovic, D.M., Cretin, B., Vairac, P.: Study on the generalized thermoelastic vibration of the optically excited semiconducting microcantilevers. Int. J. Solids Struct. **47**, 1871 (2010)
27. Lotfy, K., Abo-Dahab, S.M.: Two-dimensional problem of two temperature generalized thermoelasticity with normal mode analysis under thermal shock problem. J. Comput. Theor. Nanosci. **12**(8), 1709–1719 (2015)
28. Othman, M.I.A., Lotfy, K.: The influence of gravity on 2-D problem of two temperature generalized thermoelastic medium with thermal relaxation. J. Comput. Theor. Nanosci. **12**(9), 2587–2600 (2015)
29. Lotfy, K., Othman, M.I.A.: Effect of rotation on plane waves in generalized thermo-microstretch elastic solid with a relaxation time. Meccanica **47**(6), 1467–1486 (2012)
30. Lotfy, K.: Effect of variable thermal conductivity during the photothermal diffusion process of semiconductor medium. Silicon **11**, 1863–1873 (2019)
31. Youssef, H.M., El-Bary, A.A.: Generalized thermoelastic infinite layer subjected to ramp-type thermal and mechanical loading under three theories—state space approach. J. Therm. Stress. **32**(12), 1293–1309 (2009)
32. Ezzat, M., El-Bary, A.A., Ezzat, S.: Combined heat and mass transfer for unsteady MHD flow of perfect conducting micropolar fluid with thermal relaxation. Energy Convers. Manag. **52**(2), 934–945 (2011)
33. Ezzat, M.A., El-Bary, A.A.: MHD free convection flow with fractional heat conduction law. Magnetohydrodynamics **48**(4), 503–522 (2012)
34. Ezzat, M.A., El-Bary, A.A.: Magneto-thermoelectric viscoelastic materials with memory-dependent derivative involving two-temperature. Int. J. Appl. Electromagn. Mech. **50**(4), 549–567 (2016)
35. Song, Y.Q., Bai, J.T., Ren, Z.Y.: Study on the reflection of photothermal waves in a semiconducting medium under generalized thermoelastic theory. Acta Mech. **223**, 1545–1557 (2012)
36. Othman, M.I.A., Marin, M.: Effect of thermal loading due to laser pulse on thermoelastic porous medium under G-N theory. Results Phys. **7**, 3863–3872 (2017)
37. Rekhi, S., Tempere, J., Silvera, I.F.: Temperature determination for nanosecond pulsed laser heating. Rev. Sci. Instrum. **74**(8), 3820–3825 (2003)
38. Anzellini, S., Boccato, S.: A practical review of the laser-heated diamond anvil cell for university laboratories and synchrotron applications. Crystals **10**(6), 459 (2020)

39. Pasternak, S., Aquilanti, G., Pascarelli, S., Poloni, R., Canny, B., Coulet, M.-V., Zhang, L.: A diamond anvil cell with resistive heating for high pressure and high temperature x-ray diffraction and absorption studies. Rev. Sci. Instrum. **79**(8), 085103 (2008)
40. Yilbas, B.S., Al-Dweik, A.Y., Al-Aqeeli, N., Al-Qahtani, H.M.: Laser Pulse Heating of Surfaces and Thermal Stress Analysis. Verlag: Springer International Publishing, Heidelberg (2014)
41. Todorovic, D.M.: Plasma, thermal, and elastic waves in semiconductors. Rev. Sci. Instrum. **74**, 582 (2003)
42. Vasilev, A.N., Sandomirskii, V.B.: Photoacoustic effects in finite semiconductors. Sov. Phys. Semicond. **18**, 1095 (1984)
43. Cattaneo, C.: A form of heat-conduction equations which eliminates the paradox of instantaneous propagation. C. R. **247**, 431–433 (1958)
44. Vernotte, P.: Les paradoxes de la theorie continue de l'equation de lachaleur. C. R. **246**, 3154–3155 (1958)
45. Vernotte, P.: Some possible complications in the phenomena of thermal conduction. C. R. **252**, 2190–2191 (1961)
46. Abouelregal, A.E.: Two-temperature thermoelastic model without energy dissipation including higher order time-derivatives and two phase-lags. Mater. Res. Express **6**, 116535 (2019)
47. Zenkour, A.M., Abouelregal, A.E.: Effect of temperature dependency on constrained orthotropic unbounded body with a cylindrical cavity due to pulse heat flux. J. Therm. Sci. Technol. **10**(1), JTST0019–JTST0019 (2015)
48. Honig, G., Hirdes, U.: A method for the numerical inversion of Laplace transform. J. Comp. Appl. Math. **10**, 113–132 (1984)
49. Tzou, D.Y.: Macro-To Micro-Scale Heat Transfer: The Lagging Behavior. Taylor & Francis, Abingdon (1997)
50. Abbas, I.A., Aly, K.A.: A study on photothermal waves in a semiconductor material photogenerated by a focused laser beam. J. Mol. Eng. Mater. **04**(02), 1650003 (2016)
51. Lotfy, K., Hassan, W., El-Bary, A.A., Kadry, M.A.: Response of electromagnetic and Thomson effect of semiconductor medium due to laser pulses and thermal memories during photothermal excitation. Results Phys. **16**, 102877 (2020)
52. Khamis, A.K., El-Bary, A.A., Lotfy, K., Bakali, A.: Photothermal excitation processes with refined multi dual phase-lags theory for semiconductor elastic medium. Alex. Eng. J. **59**(1), 1–9 (2020)
53. Abouelregal, A.E.: Magnetophotothermal interaction in a rotating solid cylinder of semiconductor silicone material with time dependent heat flow. Appl. Math. Mech. Engl. Ed. **42**, 39–52 (2021)
54. Alharbi, A.M., Bayones, F.S.: Generalized magneto-thermo-viscoelastic problem in an infinite circular cylinder in two models subjected to rotation and initial stress. Appl. Math. Inf. Sci. **12**(5), 1055–1066 (2018)
55. Soleiman, A., Abouelregal, A.E., Ahmad, H., Thounthong, P.: Generalized thermoviscoelastic model with memory dependent derivatives and multi-phase delay for an excited spherical cavity. Phys. Scr. **95**(11), 115708 (2020)
56. Trajkovski, D., Čukić, R.: A coupled problem of thermoelastic vibrations of a circular plate with exact boundary conditions. Mech. Res. Commun. **26**(2), 217–224 (1999)
57. Wang, X., Xu, X.: Thermoelastic wave in metal induced by ultrafast laser pulses. J. Therm. Stress. **25**(5), 457–473 (2002)

Publisher's Note Springer Nature remains neutral with regard to jurisdictional claims in published maps and institutional affiliations.